Shock detection and limiting with discontinuous Galerkin methods for Euler equations on unstructured mesh

Hao Haibing *, Yang Yong *
*** National Key Laboratory of Science and Technology on Aerodynamic Design and Research，Northwestern Polytechnical University, Xi'an 710072, China**

Keywords: *discontinuous Galerkin methods (DGM); shock detectors; Euler equations.*

Abstract

The purpose of this paper is to simulate the transonic steady-state flows with the discontinuous Galerkin finite element method which is very sensitive to the spurious oscillations. In this article, a strategy for combining the discontinuous detector and limiter is employed to suppress the spurious oscillations near such discontinuities. The discontinuous detector is based on physicical characters of shock waves which can effectively distinguish a smooth extremum and a shock wave; Limiter is followed by Barth and Jespersen's monotonic limiter which is only used to modify the solutions slope of the detected regions to ensure the solution being monotonic. Numerical simulation for both 2D and 3D Euler Equations are presented to demonstrate the accuracy of the developed discontinuous Galerkin method. The results show that the detector can effectively identify the discontinuous regions and the limiter can effectively suppress the spurious numerical oscillations. Moreover, DG method has less numerical dissipation and excellent ability to capture shocks compared with the finite volume method with the same accuracy order.

1 Introduction

Discontinuous Galerkin method (DGM) [1-3] has been widely used in computational fluid dynamics for the past few decades. Essentially, the method can be considered as a mixture of the finite volume method (FVM) and the finite element method (FEM) which combines the advantageous features of above two methods, so the method is well suitable for solving the nonlinear problems involving shocks and other discontinuities. Generally speaking, DGM have many features [2-3]: (1) The method is well suited for complex geometries since it can be applied on unstructured grid. Furthermore, this method is suitable for handling non-uniform grid. (2) The method can easily handle adaptive strategies, since refining or coarsening a grid can be achieved without considering the continuity restriction commonly associated with the conforming elements. (3) The method is highly parallelizable, as they are compact and each element is independent. Since the elements are discontinuous and the inter-element communications are minimal, domain decomposition can be efficiently employed. (4) The method has several useful mathematical properties with respect to conservation, stability, and convergence. However, DGM has been criticized for two reasons that make it computationally expensive compared to FVM: discontinuous solutions require extra degrees of freedom; consequently, the method need a large numbered of storage requirement and the method involves integration of higher-order functions, which is traditionally carried out through numerical quadrature.

Up to now, many researchers have been devoting to solve the problems involving shocks and discontinuities. Recent investigations [4-8] have identified that when using the higher-order numerical schemes solving non-linear problem may produce oscillations near discontinuous, even though the fluxes at inter-element boundaries are up-winded through the choice of an appropriate numerical flux. The spurious oscillations result in unphysical overshoots and undershoots exist near the high gradient discontinuities. In order to suppress spurious

oscillatory, several technology of slope limiter [4, 9] are researched. In one dimension, some form of total variation diminishing (TVD) limiters [10, 4] are used to stable the high-order schemes so that spurious oscillations can be avoided without destroying the high-order accuracy of the schemes, such as moment limiter. However, in multi-dimensional spaces, DGM are facing difficulties to attain degree of accuracy, especially on unstructured meshes. The troublesome part is the construction of appropriate multi-dimensional slope limiters that preserve the accuracy of the scheme. Nevertheless, it is proved that any scheme combined with a slope limiting operator that enforces a TVD condition is at most first-order accurate and such slope limiters frequently identify regions near smooth extreme as requiring limiting. This typically results in a reduction of the optimal high-order convergence rate degeneration of the solution. In recent years, many of the limiters employ the so-called "troubled cell" (TC) approach, in which "oscillatory" cells are marked first, and the solutions in these cells are re-generated to remove or reduce the oscillations satisfying certain criteria such as mean-preserving. The idea is first developed in [12], and then further extended in [13]. The TC approach is achieved through the "discontinuity detector" [11]. In this article, Based on physical characteristics of the shock detector [14] is introduced to effectively make a distinction between a smooth extremum and a shock wave. Then, the limiter is only applied in these regions identified by this shock detector in order to reduce the computational cost and maintain the high-order accuracy of the DGM. Barth–Jespersen limiter [15] is chosen to modify the solution at discontinuous region, which is proved effectively to suppress the numerical oscillations.

The remainder of this paper is organized as follows. In Section 2 the Euler equations is briefly presented. In Section 3 and Section 4, we summarize the DGM space discretization and time discretization of the Euler equations. Section 5 describes discontinuity detector and limiter. Section 6 shows the computed results for the inviscid transonic flow around a NACA0012 airfoil and ONERA M6 wing. Finally, conclusions and some possibilities for future work are given in Section 7.

2 Governing Equations

The conservative form of the compressible Euler equations describing the conservation of mass, momentum and total energy are given in vector form:

$$\frac{\partial \mathbf{u}}{\partial t} + \nabla \cdot \mathbf{F}(\mathbf{u}) = 0 \tag{1}$$

Explicitly, the state vector $\mathbf{u}$ of the conservative variables and the Cartesian components of the inviscid flux F are:

$$\mathbf{u} = \begin{pmatrix} \rho \\ \rho u_i \\ e \end{pmatrix},$$
$$\mathbf{F}(\mathbf{u}) \cdot \mathbf{n} = (\mathrm{v} \cdot \mathbf{n}) \begin{pmatrix} \rho \\ \rho u_i \\ e + p \end{pmatrix} + p \begin{pmatrix} 0 \\ n_i \\ 0 \end{pmatrix}, \tag{2}$$

where ρ is the fluid density, u_i are the fluid velocity Cartesian components, p is the pressure and e is the total energy. For an ideal gas, the equation of state relates total energy to the pressure by:

$$e = \frac{p}{\gamma - 1} + \frac{1}{2} \rho u_i^2$$

where γ = 1.4 is the ratio of specific heats.

3 Spatial Discretization

First, we discretize (1) in space using the discontinuous Galerkin method

$$V_h^p = \{\mathrm{v}_h \in L_2(\Omega) : \mathrm{v}_h |_K \in V(K), \forall K \in \tau_h\} \tag{3}$$

where τ_h is a triangulation or tetrahedron of the domain Ω and $V(K)$ is the so-called local space.

By multiplying by an arbitrary smooth function $\mathbf{v}$ and integrate by parts over an element in the domain Ω. Thereby, we obtain the weak statement of the Eq. (1)

$$\sum_{K\in\Omega}\left(\begin{array}{l}\int_K \mathbf{v}\dfrac{\partial \mathbf{u}(x,t)}{\partial t}dK - \\ \int_K \nabla\mathbf{v}\cdot\mathbf{F}(\mathbf{u}(x,t))dK+\int_{\partial K}\mathbf{v}\,\mathbf{F}(\mathbf{u})\cdot\mathbf{n}d(\partial K)\end{array}\right)=0 \quad (4)$$

In order to discretise (4), we replace the analytical solution $\mathbf{u}$ by the Galerkin finite element approximation $\mathbf{u}_h$ and the test function $\mathbf{v}$ by $\mathbf{v}_h$, where $\mathbf{u}_h$ and $\mathbf{v}_h$ both belong to the finite element space V_h.In addition, since the numerical solution $\mathbf{u}_h$ is discontinuous between element interfaces, so we must replace the flux $\mathbf{F}(\mathbf{u}_h)\cdot\mathbf{n}$ by a numerical flux function $\mathbf{H}(\mathbf{u}_h^+,\mathbf{u}_h^-,\mathbf{n})$,

$$\begin{aligned}&\int_K \mathbf{v}_h\frac{\partial \mathbf{u}_h(x,t)}{\partial t}dK-\int_K\nabla\mathbf{v}_h\cdot\mathbf{F}(\mathbf{u}_h(x,t))dK\\&+\int_{\partial K}\mathbf{v}_h\mathbf{H}(\mathbf{u}_h^+,\mathbf{u}_h^-,\mathbf{n})d(\partial K)=0\end{aligned} \quad (5)$$

This scheme is called discontinuous Galerkin method of degree *p*, or in short notation "DG (*p*) method".

In each element, the approximation solution and test function defined by the combination of n shape function ϕ_i

$$\begin{aligned}\mathbf{u}_h(t,x)&=\sum_{i=1}^{n}\mathbf{U}_i(t)\phi_i(x)\\ \mathbf{v}_h(x)&=\sum_{i=1}^{n}\mathbf{V}_i\phi_i(x)\end{aligned} \quad (6)$$

The expansion coefficients $\mathbf{U}_i(t)$ and $\mathbf{V}_i$ denote the degrees of freedom of the numerical solution and of the test function for an element. $\phi_i(x)$ is equal to basis function, which is constructed by Gram - Schmidt orthogonalization to reduce the calculation.

The semi-discrete formulation employs a local discontinuous Galerkin formulation in spatial variables within each element K

$$\begin{aligned}&\int_K \phi_i\frac{\partial \mathbf{u}_h(x,t)}{\partial t}dK-\int_K\nabla\phi_i\cdot\mathbf{F}(\mathbf{u}_h(x,t))dK\\&+\int_{\partial K}\phi_i\mathbf{H}(\mathbf{u}_h^+,\mathbf{u}_h^-,\mathbf{n})d(\partial K)=0\end{aligned} \quad (7)$$

We replace the integrals by economical Gaussian quadrature rules as

$$\begin{aligned}&\int_K\nabla\phi_i\cdot\mathbf{F}(\mathbf{u}_h(x,t))d\,K\approx\sum_{j=1}^{n}\omega_j\nabla\phi_i\cdot\mathbf{F}(\mathbf{u}_h(x,t))|K|\\&\int_{\partial K}\phi_i\mathbf{H}(\mathbf{u}_h^+,\mathbf{u}_h^-,\mathbf{n})d(\partial K)\approx\sum_{l=1}^{L}\omega_l\phi_i\mathbf{H}(\mathbf{u}_h^+,\mathbf{u}_h^-,\mathbf{n})|e|\end{aligned} \quad (8)$$

In order to simplify the calculation of the derivatives and the integrals in Eq. (7), we defined the basis functions as polynomial functions on the reference element. For iso-parametric elements, the basis functions are expressed as functions of ξ_1, ξ_2 and ξ_3, and the coordinate transformation and its Jacobian are given by:

$$\begin{aligned}x_p&=\sum_{j=1}^{M}\hat{x}_j\phi_j(\xi_1,\xi_2,\xi_3)\\ J_K(\xi_1,\xi_2,\xi_3)&=\left|\frac{\partial(x,y,x)}{\partial(\xi_1,\xi_2,\xi_3)}\right|\end{aligned} \quad (9)$$

Finally, the semi-discrete formulation becomes:

$$\begin{aligned}&\int_{\hat{K}}\phi_j\frac{\partial \mathbf{u}_h}{\partial t}|J_K|d\hat{K}-\int_{\hat{K}}\nabla\phi_j J_k^{-1}\cdot\mathbf{F}(\mathbf{u}_h)|J_K|d\hat{K}\\&+\int_{\partial\hat{K}}\phi_j\mathbf{H}(\mathbf{u}_h^+,\mathbf{u}_h^-,\mathbf{n})|J_K|d(\partial\hat{K})=0\end{aligned} \quad (10)$$

In general, when using high-order schemes to solve flow problem of complex geometry, the errors due to geometrical approximation may dominate the discretization error and pollute the solution inside the domain. Therefore, we should take into account the curvature of the solid wall. In this paper, we take the curved boundary conditions instead of the traditional non-reflecting boundary condition [17], which can improve the accuracy without using the curve-sided elements on wall boundary.

Notice that Eq. (10), the numerical flux function $\mathbf{H}(\mathbf{u}_h^+,\mathbf{u}_h^-,\mathbf{n})$ should satisfy consistence, monotone, Lipschitz continues and conservation. In this article, an approximate Riemann solver is used to compute the flux at inter-element boundaries. The upwind flux difference splitting schemes of Roe [16] is employed, which has less artificially dissipation and strongly ability of shock capture.

4 Time Discretization

The equations defining the approximate solution can be rewritten in ODE form as

$$M\frac{d\mathbf{U}}{dt}=R(\mathbf{U}) \tag{11}$$

where M denotes mass matrix, $\mathbf{U}$ is the global vector of the degrees of freedom, and $R(\mathbf{U})$ is the residual vector. In this paper, we use the TVD Runge-Kutta time discretization in time and the time-marching algorithm as follows:

1. set $u_h^0=P_{V_h}(u_0)$
2. For $n=0,\dots N-1$ computer u_h^{n+1} as follows:
   - Set $u_h^0=u_h^n$
   - for $i=1,\dots k+1$ computer the intermediate functions:

$$u_h^i=\left\{\sum_{l=0}^{i-1}\alpha_{il}u_h^l+\beta_{il}\Delta t^n M^{-1}R_h(u_h^l,\gamma_h(t^n+d_l\Delta t^n))\right\}$$

3. Set $u_h^{n+1}=u_h^{k+1}$.

Here, the parameters α_{il} and β_{il} are from literature [4].

5 Discontinuity Detection and Limiting

Due to high-order numerical schemes produce spurious oscillations in the vicinity of discontinuities, which can lead to numerical instabilities or unbounded solutions. In order to suppress spurious oscillatory near discontinuities without reducing the accuracy of solution, in this article, we take the technique which combining shock detector and slope limiter to eliminate the spurious oscillations.

5.1 Discontinuity Detection

A shock detector which is based on the characters of shock is introduced here, which is found to be quite helpful and effective in making a distinction between a stagnation point and a shock wave. This shock detector is based on the two main physics facts about a shock wave, namely (1) the normal Mach number is greater than 1 before a shock and less than 1 after a shock, and (2) a shock wave can only be a compressive wave. This can be easily come true using the following three steps:

1. Computer shock wave direction $\mathbf{n}$ on each element

$$\mathbf{n}=\frac{\nabla q}{|\nabla q|} \tag{12}$$

where q is the velocity vector magnitude.

2. Compute maximum and minimum normal Mach number on each element by taking flow variables at the adjacent faces into consideration.

3. Compute the following wave indicator:

$$k=\frac{\partial(\mathrm{v}\cdot\mathbf{n})}{\partial n} \tag{13}$$

Here, v is the velocity vector. For compression wave $k<0$, and for expansion wave $k>0$.

5.2 Limiting

With limiting only used near discontinuities, we need not be as concerned with maintaining a high order of accuracy, thus, we choice the curvature limiting schemes of Barth and Jespersen in multiple dimensions. Following Barth and Jespersen, slopes are limited so that the solution at the quadrature points $x_j, j=1,2,\cdots,K_{T_i}$ in each element Ω_i, $\mathbf{U}_i(\mathbf{x}_j)$ is in the range spanned by the neighboring solution averages

$$\bar{\mathbf{U}}_i^{\min}\le\mathbf{U}_i(\mathbf{x}_j)\le\bar{\mathbf{U}}_i^{\max} \tag{14}$$

where $\bar{\mathbf{U}}_i^{\min}$ and $\bar{\mathbf{U}}_i^{\max}$ are the minimum and maximum element averaged solution on the elements sharing faces with Ω_i. If (14) is violated for any quadrature points, then it is assumed that the element is close to a discontinuity, and the solution at this element Ω_i is locally modified as

$$\mathbf{U}_i(\mathbf{x})=\bar{\mathbf{U}}_i+\alpha\nabla\mathbf{U}_i\cdot(\mathbf{x}-\mathbf{x}_i)\quad\forall\mathbf{x}\in\Omega_i \tag{15}$$

where $\bar{\mathbf{U}}_i$ is the cell-averaged solution at the element Ω_i, $\mathbf{x}_i$ is the position vector of the centroid of Ω_i,and

$$\alpha=\min_{1\le j\le K_{\Gamma_i}}\alpha_j \tag{16}$$

Where,

$$\alpha_j = \begin{cases} \min(1, \dfrac{\bar{\mathbf{U}}_i^{\max} - \bar{\mathbf{U}}_i}{\mathbf{U}_i(\mathbf{x}_j) - \bar{\mathbf{U}}_i}) & if\ \mathbf{U}_i(\mathbf{x}_j) - \bar{\mathbf{U}}_i > 0 \\ \min(1, \dfrac{\bar{\mathbf{U}}_i^{\min} - \bar{\mathbf{U}}_i}{\mathbf{U}_i(\mathbf{x}_j) - \bar{\mathbf{U}}_i}) & if\ \mathbf{U}_i(\mathbf{x}_j) - \bar{\mathbf{U}}_i < 0 \\ 1 & otherwise \end{cases} \tag{17}$$

For $p > 1$, we set the higher-order coefficients in (6) to zero and apply (15) to the remaining solution whenever $\alpha \neq 1$ .Applying limiting to characteristic variables may produce negative pressures; thus, rendering the solution unstable. Should such nonphysical solutions result, we set $\mathbf{U}_i = \bar{\mathbf{U}}_i$.

6 Numerical Results and Discussions

The first example is the transonic flow past a NACA0012 airfoil at a Mach number of 0.8, at 1.25° attack angle with the mesh shown in Fig. 1. The mesh has 1861 elements, 2207 grid points, and 101 boundary points. Fig.2 displays comparison of airfoil pressure coefficients between FVM and DGM (p=1). The pressure contours and the detected regions are shown in Fig 3, where we can obviously see that the detected regions located in the discontinuous vicinity. Fig.4 shows the iso-Mach contours.

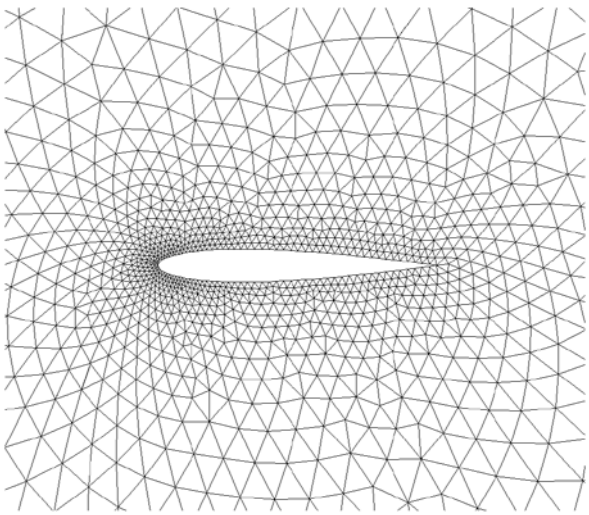

Fig. 1 NACA0012 airfoil computational grid

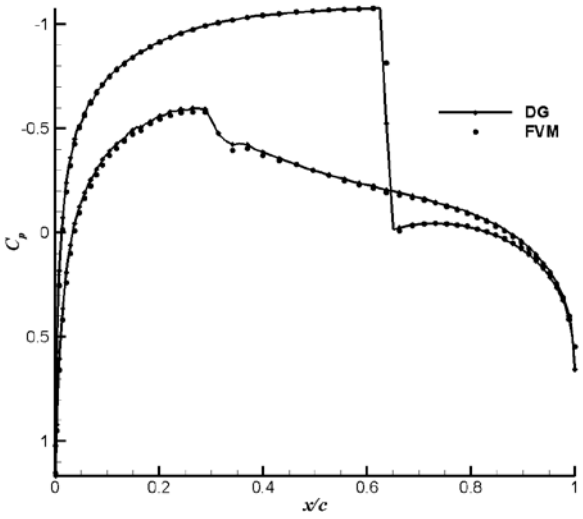

Fig.2 Comparison of airfoil pressure coefficients

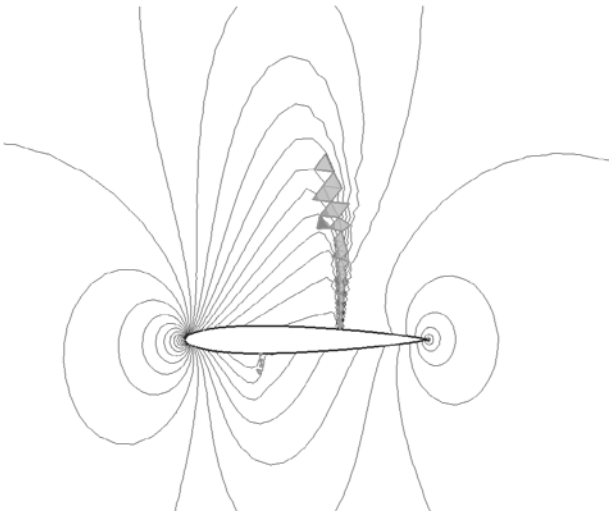

Fig.3 Contour of pressure of naca0012 field and detected regions

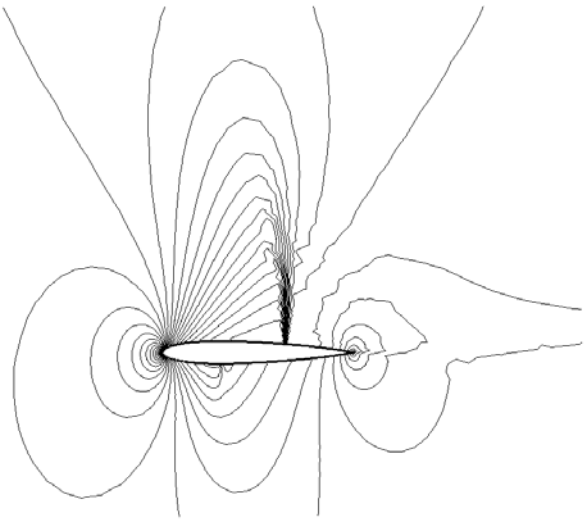

Fig.4 Contour of Mach number

Another example is the transonic flow over the M6 wing at a Mach number of 0.84, at 3.06^{o} attack angle with surface mesh shown in Fig.5. The whole mesh includes 21019 elements, 99350 points. The computed pressure contours on the upper wing surface obtained by the method is shown in Fig.6. The upper surface contours clearly show the sharply captured lambda-type sock structure formed by the two inboard shock waves, which merge together near 87% semi-span to form the single strong shock wave in the outboard region of the wing. The computed pressure coefficient distributions obtained by DG (p=1) and FVM are compared at six span-wise stations in Fig.7, where experimental data for the pressure coefficients are also given as a reference. In these figures, the two curves are compared closely with experimental data. However, DGM capture more sharp shocks and capture the suction peak greater at the leading edge than FVM.

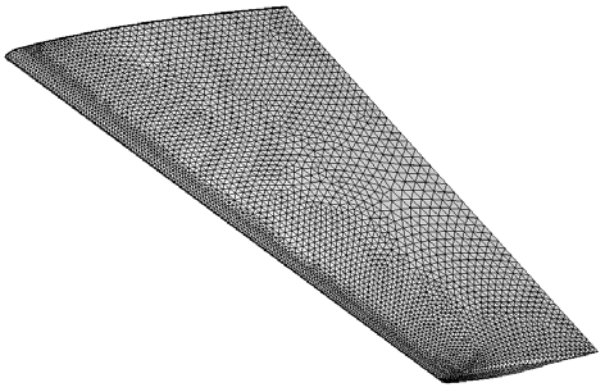

Fig.5 M6 wing computational grid

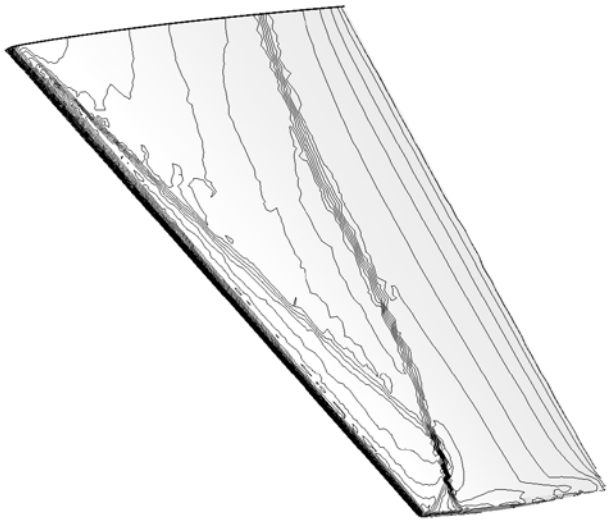

Fig.6 Isoline of pressure on an the upper surface on M6 wing

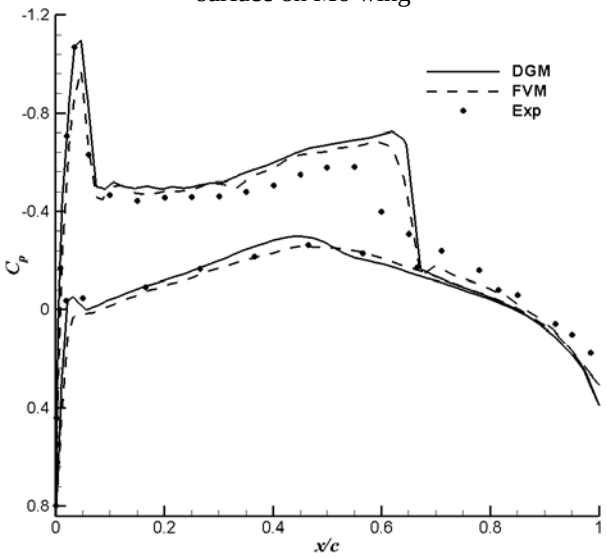

(a) η =20%

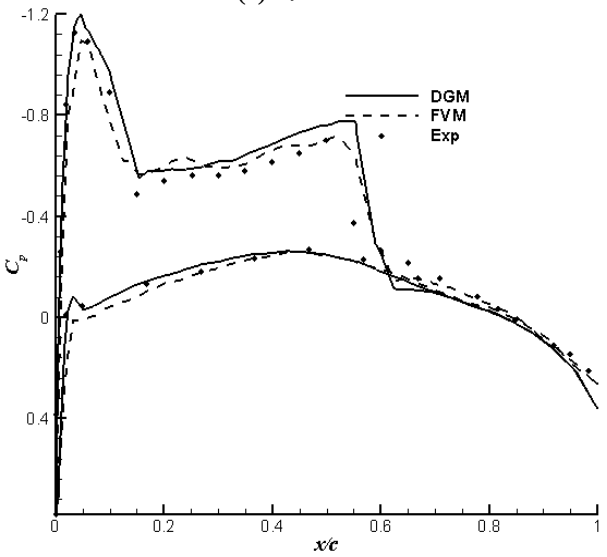

(c) η = 44%

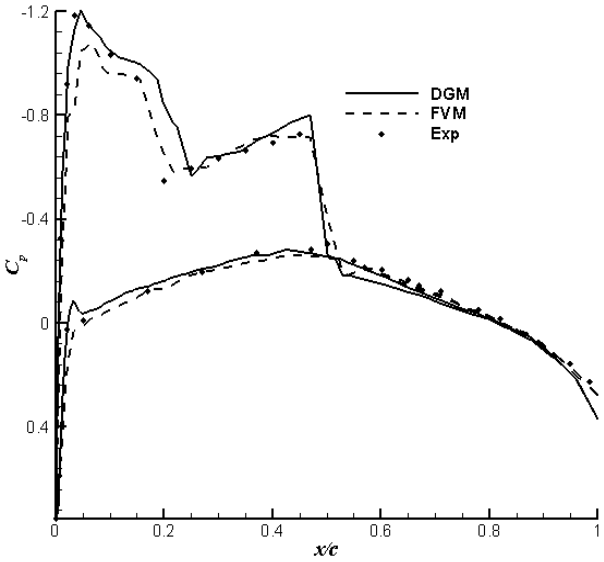

(e) η = 65%

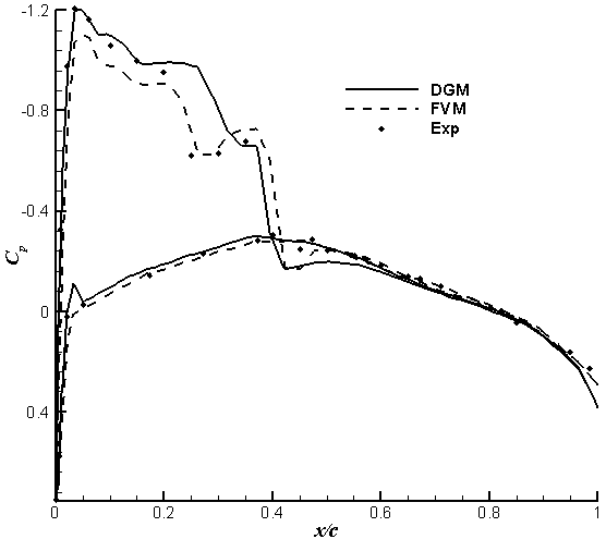

(b) η = 80%

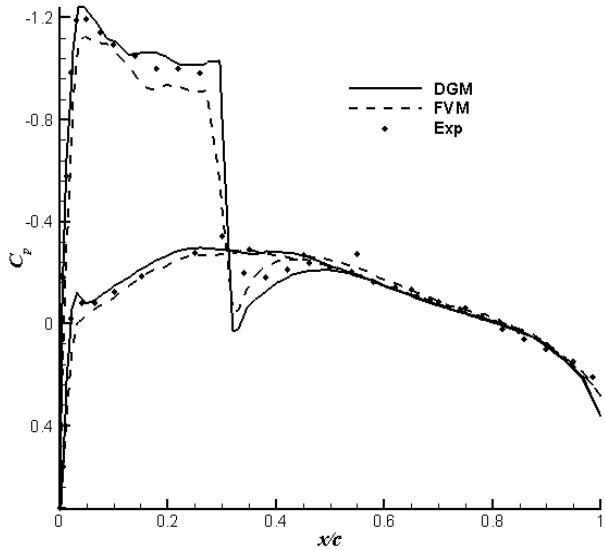

(d) η = 90%

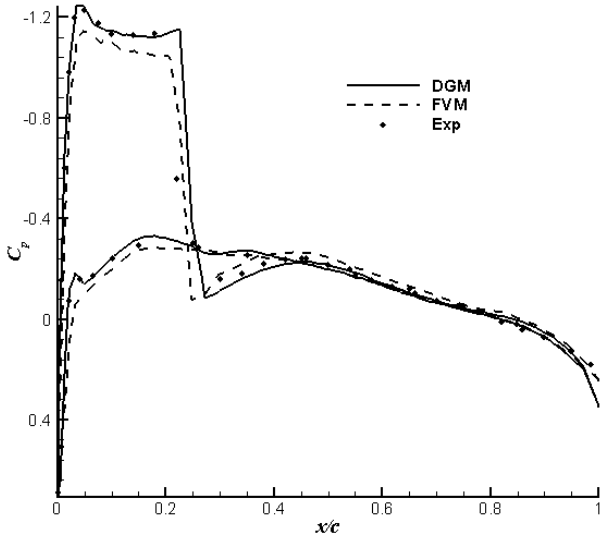

(f) η = 95%

Fig.7 The chord-wise Cp distribution at different span-wise locations of M6 wing ((a)-(f))

7 Conclusions

In this paper, a new method has been established for the discontinuous Galerkin method to suppress overshoots and undershoots in the simulation of transonic compressible flows. The method that combines shock detector and slope limiter is proved to be effective by two numerical examples. The results show that the method can eliminate the spurious oscillations near discontinuities, and compared with the finite volume method with the same accuracy order, it has less numerical dissipation and excellent ability to capture shocks.

At present, the method is applied to the DGM (p=1). For high-order DGM (p>1), it remains to be investigated in the future work.

7 References

[1] Bassi F, Rebay S. High-order accurate discontinuous finite element solution of the 2D Euler equations. Journal of Computational Physics 1997; 138:251–285.

[2] Cockburn B, Hou S, Shu CW. TVD Runge–Kutta local projection discontinuous Galerkin finite element method for conservation laws IV: the multidimensional case. Mathematics of Computation 1990; 55:545–581.

[3] B. Cockburn and Chi-Wang Shu. Runge-Kutta Discontinuous Galerkin Methods for Convection-Dominated Problems [J]. Journal of Scientific Computing, Vol. 16, No. 3, September 2001.

[4] L.Krivodonova. Limiters for high-order discontinuous Galerkin methods, J. Comput. Phys., 226 (2007), pp. 879–896.
[5] H. Luo, J. D. Baum And R. Lohner. A Hermite Weno-based limiter for discontinuous Galerkin method on unstructured grids, J. Comput. Phys., 225 (2007), pp. 686–713.
[6] J. Qiu And C-W. Shu. Hermite WENO schemes and their application as limiters for Runge-Kutta discontinuous Galerkin method: one-dimensional case, J. Comput. Phys., 193 (2003), pp.115–135.
[7] S. Adjerid, K. Devine, J. Flaherty, L. Krivodonova. A posteriori error estimation for discontinuous Galerkin solutions of hyperbolic problems, Comput. Methods Appl. Mech. Engrg. 191 (2002) 1097–1112.
[8] J. Flaherty, L. Krivodonova, J.-F. Remacle, M. Shephard. Aspects of discontinuous Galerkin methods for hyperbolic conservation laws, Finite Elements Anal. Design 38 (2002) 889–908.
[9] J. Goodman, R. LeVeque. A geometric approach to high resolution TVD schemes, SIAM J. Numer. Anal. 25 (1988) 268–284.
[10] B. Van Leer, Towards the ultimate conservative difference scheme V. a second order sequel to Godunov's method, J. Comput. Phys., 32 (1979), pp. 101–136.
[11] J. Qiu And C-W. Shu. A comparison of troubled-cell indicators for Runge-Kutta discontinuous Galerkin Methods using weighted essentially nonoscillatory limiters, SIAM J. Sci. Comput. 27 (2005).
[12] B. Cockburn And C-W. Shu. TVB Runge-Kutta local projection discontinuous Galerkin finite element method for conservation laws II: general gramework, Math. Comput., 52 (1989),pp. 411–435.
[13] R. Biswas, K. D. Devine And J. Flaherty. Parallel, adaptive finite element methods for conservation laws, Appl. Numer. Math., 14 (1994), pp. 255–283.
[14] Hong Luo, Joseph D.Baum and Rainald L $^{\ddot{o}}$ hner. On the computation of steady-state compressible flows using a discontinuous Galerkin method, Int. J. Numer. Meth. Engng 2008; 73:597–623.
[15] Timothy J. Barth and Dennis C. Jespersen. The Design of Application of Upwind Schemes on Unstructured Grids, AIAA-89-0366.
[16] P. Roe. Approximate Riemann Solvers, Parameter Vectors, and Difference Schemes, Journal of Computational Physics, vol. 43, pp. 357-372, 1981.
[17] ZJ. Wang and Yuzhi Sun. A Curvature-based Wall Boundary Condition For The Euler Equation On Unstructured Grids, AIAA 2002-0966.

Copyright Statement